New measurement of the proton capture rate on ^{7}Be and the $S_{17}(0)$ factor

L. T. Baby,[1] C. Bordeanu,[1,*] G. Goldring,[1] M. Hass,[1] L. Weissman,[2] V. N. Fedoseyev,[3] U. Köster,[3] Y. Nir-El,[4] G. Haquin,[4] H. W. Gäggeler,[5] R. Weinreich,[5] and the ISOLDE Collaboration

[1]*Department of Particle Physics, Weizmann Institute of Science, Rehovot, Israel*

[2]*NSCL, Michigan State University, East Lansing, Michigan 48824*

[3]*ISOLDE, CERN, Geneva, Switzerland*

[4]*Soreq Research Centre, Yavne, Israel*

[5]*Paul Scherrer Institute, Villigen, Switzerland*

(Received 11 December 2002; published 23 June 2003)

The ^{7}Be$(p,\gamma)^8$B reaction plays a central role in the evaluation of solar neutrino fluxes. We report on a new precision measurement of the cross section of this reaction, following our previous experiment with an implanted ^{7}Be target, a raster-scanned beam, and the elimination of backscattering losses. The new measurement incorporates a higher activity ^{7}Be target and a number of improvements in design and procedure. The cross section at a selected energy $E_{\text{c.m.}}=850$ keV (where c.m. stands for center of mass) was measured several times under varying experimental conditions, yielding a value of $S_{17}(E_{\text{c.m.}}=850\ \text{keV})=24.0\pm0.5$ eV b, to serve as a benchmark. Measurements were carried out at lower energies as well. Due to the precise knowledge of the implanted ^{7}Be density profile, it was possible to reconstitute both the off- and on-resonance parts of the cross section and to obtain from the entire set of measurements an extrapolated value of $S_{17}(0)=21.2\pm0.7$ eV b, using the cluster model of Descouvemont and Baye.

DOI: 10.1103/PhysRevC.67.065805 PACS number(s): 25.40.Lw, 26.65.+t, 26.20.+f, 27.20.+n

I. INTRODUCTION

The study of fusion reactions in the Sun, relevant to the observed solar neutrino shortfall, has been the subject of intensive research, reviewed in Refs. [1,2]. Recently, this subject has acquired additional significance with the new results of the Super-Kamiokande [3] and SNO [4] experiments, demonstrating the existence of neutrino oscillations. The ^{7}Be$(p,\gamma)^8$B reaction and the accurate determination of the astrophysical $S_{17}(0)$ factor is of great importance to the solar neutrino issue and to other related astrophysical studies [5–7] since ^{8}B is the source of the high-energy neutrinos from the Sun that are detected in the SNO, Kamiokande, and Homestake [8] experiments.

The direct capture cross sections are measured at high energies compared to the solar energies (20 keV) and extrapolated to ''zero'' energy using an energy-dependent parametrization. The quantity used for the extrapolation is the astrophysical S factor $S(E)$ that varies slowly with energy compared to the cross section $\sigma(E)$. $S(E)$ is related to $\sigma(E)$ by the relation

$$S(E)=E\sigma(E)\exp[2\pi Z_1 Z_2 e^2/\hbar v], \tag{1}$$

where Z_1, Z_2 are the atomic numbers and v the relative velocity.

The most widely used method of obtaining the cross section for the ^{7}Be$(p,\gamma)^8$B reaction is by direct measurement of capture of protons on a ^{7}Be target and the detection of the β-delayed α particles from the decay of ^{8}B (see Ref. [1] and references therein). A direct measurement of the cross section has also been carried out with the kinematically inversed reaction ^{1}H(^{7}Be, $\gamma)^8$B [9], albeit with limited statistical accuracy. There are also on record various non direct measurements of S_{17}, which can be categorized as (a) Coulomb breakup of ^{8}B in the time-dependent electromagnetic field of a high-Z target [10–12] and (b) peripheral reactions which are amenable to the ANC (asymptotic normalization coefficient) treatment [13–16]. These methods, as stated in the papers above and also in a recent paper of indirect methods [17], are still subject to uncertainties related to the model dependence of the extracted S-factor values.

In previous papers [18,19] we have demonstrated a new method for measuring the cross section of the ^{7}Be$(p,\gamma)^8$B reaction by overcoming several of the recognized potential systematic errors in earlier measurements (see, e.g., Ref. [1]). Our method involves a small diameter implanted ^{7}Be target from ISOLDE (CERN) and a raster-scanned beam over an area larger than the target spot, avoiding the difficulties encountered with targets of nonuniform areal distribution. The implanted target also eliminates the backscattering loss of ^{8}B. Several experiments [20–22] have recently been published, quoting $S_{17}(0)$ values of 3–10 % accuracy, two of those [21,22] using methods similar to Ref. [19]. However, there still exist large, up to 20%, discrepancies among experimental results as well as the extracted $S_{17}(0)$ values of these measurements. The present work has been undertaken in order to address these discrepancies and to provide a new, firm input for the determination of this cross section by exploiting fully the advantages of the implanted target: full knowledge of the target composition and the ^{7}Be profile, target robustness, and the ability to produce a secondary target of reduced activity to improve the conditions for the γ calibration of the target. Another feature of the present work is a thin α detector and relatively small solid angles, providing clean α spectra.

*On leave from Horia Hulubei-National Institute for Physics and Nuclear Engineering, Bucharest-Măgurele, Romania.

A brief account of this work has been published elsewhere [23]. Here we present the full details of the experiment and analysis, and a comparison to other recent results.

II. EXPERIMENT AND PROCEDURE

The general scheme of the experiment follows that of our previous publications [18,19]. We repeat here for convenience some sections of Ref. [19] with suitable changes and additions. The main feature of this measurement is the use of a small size target, implanted into a low-Z material and a uniformly scanned particle beam larger than the target. In general, and as described in Ref. [18], the reaction yield is given by

$$Y=\sigma\int\frac{dn_{\mathrm{b}}}{dS}\frac{dn_{\mathrm{t}}}{dS}dS, \tag{2}$$

where n_b, n_t are the total numbers of beam and target particles, respectively, and dn_b/dS, dn_t/dS are areal densities.

When the target is known to be uniform and the beam is smaller than the target, Eq. (2) can be simplified to the familiar relation

$$Y=\sigma\frac{dn_t}{dS}\int\frac{dn_b}{dS}dS=\sigma\frac{dn_t}{dS}n_b.$$

In such a case, the evaluation of the cross section depends only on the total beam flux. However, for targets of nonuniform areal distribution, e.g., radiochemically prepared ^{7}Be targets [24], the full relation (2) has to be used in the evaluation. The inherent uncertainties in the distributions dn_{b}/dS and dn_{t}/dS may lead to considerable uncertainties in the value of the integral and hence in the deduced cross section. We have addressed this problem by reversing the arrangement: we use a homogeneous beam—produced by raster scanning—impinging on a target smaller than the beam. Relation (2) then reduces to

$$Y=\sigma\frac{dn_b}{dS}n_t, \tag{3}$$

requiring only a determination of the total number of target nuclei and of the areal density of the beam.

The general scheme of the experiment is shown in Fig. 1. A proton beam from the Weizmann Institute 3-MV Van de Graaff accelerator is raster scanned over a rectangle of 4.5 $\times$3.5 mm^2. The purpose of the scan is to obtain a beam of uniform areal density, as demonstrated in detail in Refs. [18,25]. The scanned proton beam is collimated by a 3-mm-diameter hole and impinges on the ^{7}Be target of 2 mm diameter. A liquid nitrogen cooled cryofinger is placed close to the target area to protect the target surface from contamination. A vacuum of $\approx 6\times10^{-7}$ mbar was maintained in the chamber. The target spot is aligned with a set of interchangeable collimators downstream from the target. The target is mounted on an arm that is periodically rotated by a microstepping motor out of the beam and in front of a silicon surface barrier detector, registering the delayed α's following the β decay of ^{8}B. In the present experiment a 150-mm^2, 25-μm silicon surface barrier detector was used, which provided a sufficiently thick depletion layer to stop the α particles from the reaction but minimized the interaction with γ rays from the ^{7}Be activity. The detector was mounted at distances of 7–10 mm from the target.

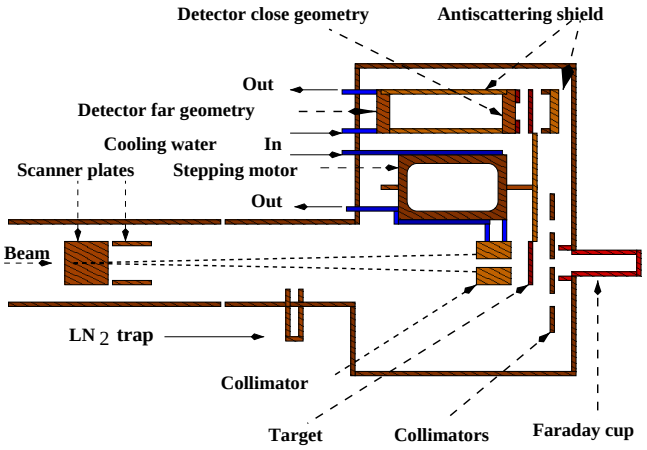

FIG. 1. A schematic view of the experimental setup.

The time sequence of the entire cycle is 1.5 s beam on target, 100 ms rotation, 1.5 s target in the counting position, 100 ms rotation back to the beam position. The detection efficiency [26] resulting from the known lifetime of ^{8}B and this cycle is $\eta_{\mathrm{cycle}}=0.390\pm0.001$. In the counting position a signal from the motor control unit enables an ADC for α counting and the gated scaler for Faraday-cup beam monitoring. In the beam-on-target position, a second ADC is enabled for background counting.

In terms of the experimental parameters, the cross section of the reaction $^7\mathrm{Be}(p,\gamma)^8\mathrm{B}\rightarrow{}^8\mathrm{Be}\rightarrow 2\alpha$ can be written as

$$\sigma(E_{\mathrm{c.m.}})=\frac{N_\alpha}{n_t}\left(\frac{A}{N_p}\right)\frac{1}{\eta_{\mathrm{Be}}\eta_{\mathrm{cycle}}}, \tag{4}$$

where N_α is the number of measured α particles, N_p/A is the integrated current density through a collimator hole of area A, and η_{Be} is the geometrical detection efficiency of the reaction products (see Sec. II F), which is twice the detection efficiency of α's.

A. The implanted target

The ^{7}Be target was prepared at the ISOLDE (CERN) in a manner similar to that described in Ref. [19] by direct implantation of ^{7}Be at 60 keV in a copper disk of 12 mm diameter and 1.5 mm thickness. The main novel feature was the primary source of ^{7}Be for ISOLDE: a graphite target from the Paul Scherrer Institute (PSI) [27], used routinely at PSI for the production of π mesons. A large number of spallation products is accumulated in the target, including ^{7}Be. A fraction of this graphite target was placed inside an ISOLDE target container and brought to ISOLDE for an off-beam implantation using a resonance ionization laser ion source. The laser ionizes ^{7}Be selectively, but ^{7}Li (present copiously in the target) is also selected as a part of the mass selected ($A=7$) beam; ^{7}Li is surface ionized in the hot tungsten cav-

ity due to its low ionization potential. The ratio of ^{7}Be to ^{7}Li can be measured by switching off the laser, leaving only the ^{7}Li ions. The initial ^{7}Li current was quite high (of the order of 100–200 nA) but after heating the source for a few hours, the ^{7}Li current dropped considerably and an almost pure beam of ^{7}Be (40–90 nA) was obtained. The average ^{7}Li/^{7}Be ratio during implantation was ≈ 0.08. Subsequent, more precise measurements of the ^{7}Li content yielded a value of 0.11 for this ratio at $t=0$, the end of implantation on 6 December, 2001.

The implantation was carried out in a way that provided full control of the numbers of implanted ^{7}Be and ^{7}Li as we all a determination of the areal density of the implanted ions. The total number of implanted ions was determined by recording the integrated charge of beam on target, and the ratio ^{7}Li/^{7}Be was determined by repeated measurements of the ion current with the laser ''on'' and ''off.''

Credible current measurements depend on Faraday cups or other means of secondary-electron suppression, all requiring several centimeters of space between the defining collimator and the target. The postulated sharp and accurate definition of the target spot dictates, on the other hand, close proximity of the defining collimator to the target. This problem was solved in an implantation chamber shown schematically in Fig. 2(a). The chamber contains two equipotential regions: region 1, the first along the beam, has an iris diaphragm with an opening radius r of 0.9–6.0 mm and attached to it a Faraday cup. Region 2 contains the target button: a copper disk 12 mm in diameter and 1.5 mm thick, pressed against a thin steel plate with a 2-mm-diameter hole in the center, the defining collimator. This assembly is in turn pressed against the frame of the iris diaphragm with an intervening thin insulating ring.

Secondary electrons from the ions hitting the iris at opening r, $n_i(r)$, are collected in the Faraday cup at the same potential, and such ions are therefore recorded faithfully. Secondary electrons from the $n_t(r)$ ions hitting the target assembly are also collected in region 1, and they enhance the current readings from region 2 and diminish by the same amount the current readings from region 1. If we denote $I_i(r)$ and $I_t(r)$ as the integrated currents from the two regions, and α as the secondary emission coefficient, we have

$$I_i(r)=n_i(r)-\alpha n_t(r), \qquad I_t(r)=(1+\alpha)n_t(r),$$

$$I_i(r)+I_t(r)=n_i(r)+n_t(r)=n_T,$$

n_T being the total number of ions in the beam. Figure 2(b) shows the measured $I_i(r)$ and $I_t(r)$. The dashed lines are fits to the points with functions $I_t(r)=I_t(\infty)[1-\exp(-r^2/a^2)]$, and $I_i(r)=n_T-I_t(r)$, with $n_T=7.5$ and $a^2=1.3$ mm^2. The areal density of the ^{7}Be beam, $\rho(r)$, and *ipso facto* of the target can be computed as $\rho(r)=\rho(0)\exp(-r^2/a^2)$, which is shown in Fig. 3 (bottom).

The recording of implanted ions is carried out in two steps: (a) from the profile measurement one gets for $r=1$ mm,

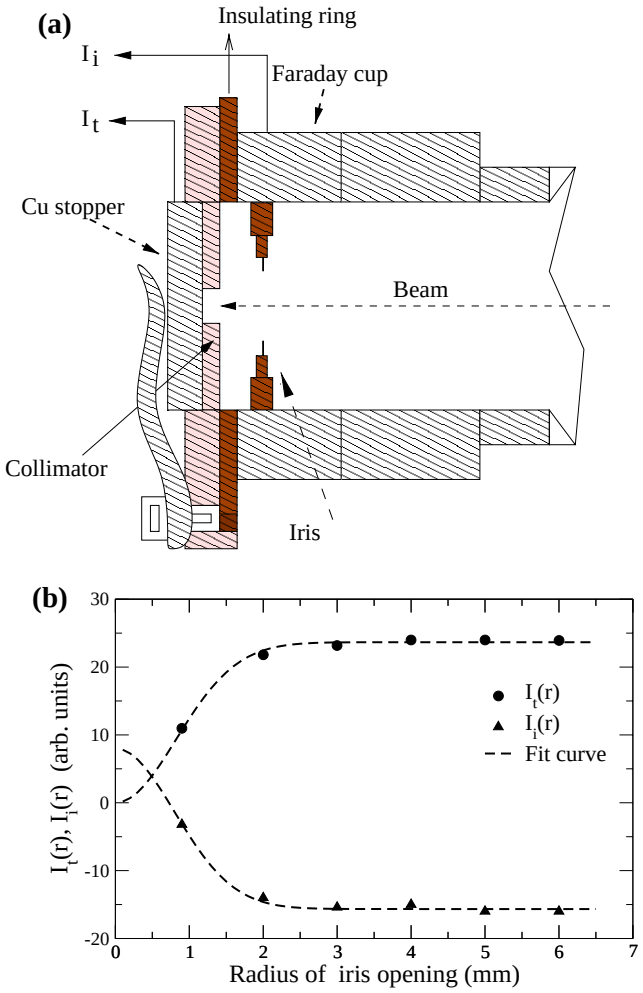

FIG. 2. (a) A schematic view of the implantation chamber. Note the collimator of 2 mm diameter in the beam path that defines the dimensions of the ^{7}Be spot. (b) The measured beam profiles as function of the iris opening.

$$R=\frac{I_t(1)}{I_t(\infty)}=\frac{(1+\alpha)n_t(1)}{(1+\alpha)n_t(\infty)}=\frac{n_t(1)}{n_T},$$

R was measured to be $R=0.63\pm 0.1$; (b) during the implantation the sum of $I_i(r)$ and $I_t(r)$ was measured with a large opening and integrated, yielding the number of ^{7}Be ions collected in a disk of 1 mm radius at the end of implantation ($t=0$):

$$n_t(1)=n_T\times\frac{I_t(1)}{I_t(\infty)}=(1.18\pm 0.12)\times 10^{16}.$$

The precise determination of the number of ^{7}Be using γ counting (see Sec. II D) yielded the value $(1.168\pm 0.008)\times 10^{16}$ for this quantity.

The implanted ^{7}Be target has a number of important advantages:

(1) The implantation profile is known from simulation and from a direct secondary ion mass spectrometry measurement for ^{9}Be implanted in Cu [19]. Figure 3 (top) shows the density distribution of 60 keV ^{7}Be's implanted in copper. One

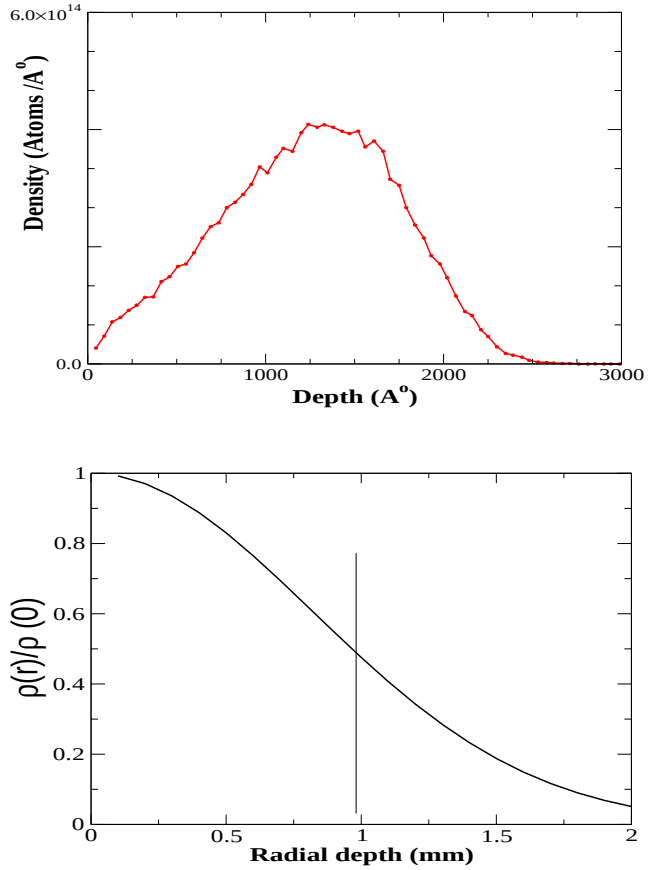

FIG. 3. Top: The simulated depth distribution of 60-keV ^{7}Be in copper. Bottom: The areal density distribution of ^{7}Be beam used for implantation at the ISOLDE; this is also the ^{7}Be density distribution in the target. The vertical line indicates the edge of the implanted target. (see Sec. II A for details.)

parameter of this simulation—the depth of the centroid of the distribution—has now also been confirmed in the present measurement (see Sec. II K). The knowledge of the composition and the ^{7}Be density profile is important for evaluating the backscattering loss of ^{8}B's from the target. We computed the ^{8}B backscattering loss to be 0.2%, small enough to be ignored. The areal distribution of ^{7}Be in the target is also known [Fig. 3 (bottom)].

(2) The elemental composition of the target is known precisely; the target consists of Cu, ^{7}Be, and ^{7}Li. We had immediately after implantation ($t=0$) 1.17×10^{16} ^{7}Be atoms and 10^{15} ^{7}Li atoms in a cylindrical volume of copper, 2 mm in diameter and 2500 Å deep, containing a total of 6.7×10^{16} Cu atoms. The majority of the ^{7}Li atoms during the time of the experiment were β-decay daughters of ^{7}Be, and they have the same density profile.

(3) The target is robust. We have direct evidence that both the ^{7}Be and ^{7}Li atoms remained stable in the Cu matrix throughout the duration of the experiment (see Sec. II K), with the exception of singular event—"the thermal episode" to be described later.

(4) The target is calibrated for ^{7}Be content by monitoring the γ rays following the $^{7}\mathrm{Be}\rightarrow{}^{7}\mathrm{Li}\beta$ decay. The γ measurements carried out in standard counting arrangements require

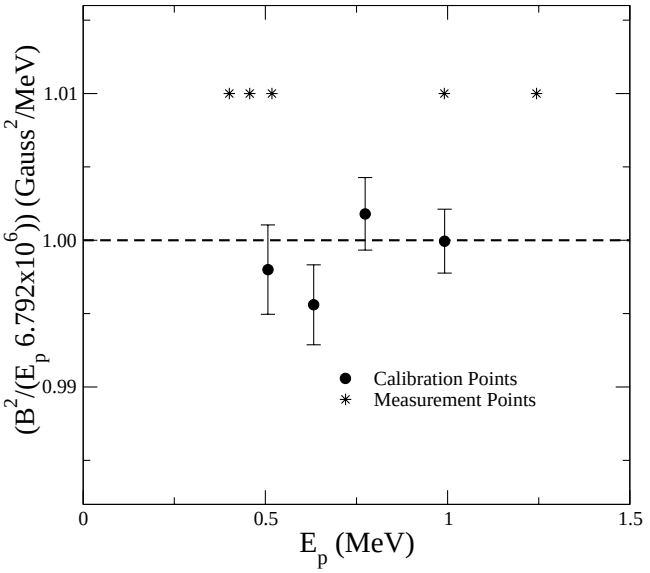

FIG. 4. Energy calibration of the Van de Graaff accelerator. The circles represent the calibration points and the asterisks represent the energies at which $^{7}\mathrm{Be}(p,\gamma)^{8}\mathrm{B}$ measurements were carried out. The constant $(6.79\pm0.02)\times10^{6}$ G^2/MeV used to scale the y axis is obtained from the fit as described in the text (Sec. II B).

the γ activity of the sample to be below a limit much smaller than the actual activity of our target. With the implantation technique it was possible to produce for the purpose of calibration a secondary target about 300 times weaker than the primary target, identical to it in all other aspects (cf. Sec. II D).

Based on the geometrical parameters of the target [Fig. 3 (bottom)] one can estimate the sensitivity of the cross section measurements to beam inhomogeneity. Assuming a target distribution e^{-r^2/a^2} and a beam distribution e^{-r^2/b^2}, one can compute the ratio X_R of the true cross section as computed from Eq. (2) to the value obtained with the procedure of Eq. (4). For example, with $a^2=1.3$ mm^2 and $b^2>0.5$ one gets to a good approximation: $X_R=1+(0.06/b^2)$. This implies a rather low sensitivity to beam inhomogeneity. In an extreme case of $b^2=a^2=1.3$ mm^2, one gets $X_R=1.05$. One can also well account in this way for the seemingly low reduction in the value of N_α/CI when the beam scan is switched off (Fig. 5).

B. Proton energy calibration

The proton energy of the Van de Graaff accelerator was calibrated with the $^{27}\mathrm{Al}(p,\gamma)^{28}\mathrm{Si}$ resonances at energies of 991.2, 773.7, 632.6, and 504.9 keV. The calibration curve for the accelerator is shown in Fig. 4. The constant $B^2/E_p=(6.79\pm0.02)\times10^{6}$ G^2/MeV, where B is the field of the analyzing magnet, is seen to be in excellent agreement with all the measured points and has been used to establish intermediate points of E_{lab} as well as lower values, down to $E_{\mathrm{lab}}=430$ keV and one higher point at $E_{\mathrm{lab}}=1244$ keV.

C. Beam uniformity

The scanned beam density dn_b/dS, typically of about 0.3–0.5 μA/mm^2 was measured by integrating the beam in

an electron suppressed Faraday cup after passing through a 2-mm-diameter aperture. The current was digitized and recorded in a gated scaler. Beam integration with and without suppression yielded results similar to within a fraction of 1%. The beam uniformity was checked as in Ref. [18], by measuring the α yield N_α from the ^{7}Li$(d,p)^8$Li reaction versus integrated current (CI) for three downstream collimators with nominal diameters 2, 1.5, and 1 mm. Figure 5 shows the measured $(N_\alpha/CI)A$. The constancy of this quantity for the different collimators attests the constancy of the average number of beam particles (deuteron) in the circular area of the beam (see also Sec. II F). To obtain the optimum scan voltage, the α yield from the ^{7}Li$(d,p)^8$Li reaction at $E_d=770$ keV was measured as a function of scan voltage [Fig. 5(top)]. This procedure was repeated at a lower energy (470 keV) also to obtain the corresponding scan voltage. A correction was applied to the measured beam density for the finite distance between the target and the beam collimator and the diverging beam from the scanner plates. The beam collimator was positioned 10 mm behind the target and the scanning plates to target distance was 140 cm, yielding a correction factor of 1.014.

D. Target calibration

The ^{7}Be content was determined as in Ref. [19] by a measurement of the γ activity of the target using known values of the branching ratio of the ^{7}Be β decay to the first excited state of ^{7}Li and the ^{7}Be half-life. The γ activity of the ^{7}Be target was too intense to be assayed in a standard γ-calibration setup due to the problems associated with large dead times in the γ counting. As stated above, a weak target was prepared for γ calibration. An accurate measurement of the relative intensities of the ^{7}Li 478-keV γ transition for the two targets was carried out at the low background γ counting laboratory of NRC-Soreq by placing both at the same distance from a Ge counter, yielding a ratio of 317.8 ± 0.8. This ratio was remeasured several times with consistent results. The absolute intensity of the weak target was measured at the NRC-Soreq laboratory and also at the Texas A&M University. Both measurements followed calibration procedures involving up to 13 high-precision standard sources of 10 radionuclides. The Texas A&M measurement also incorporated a precise ^{60}Co source (0.1% error on its absolute activity) and Monte Carlo calculations which agreed to within 0.2% with all measured data from 50 to 1500 keV for interpolating between measurements [28]. The two measurements yield a ^{7}Be content for the weak target of $(2.667\pm0.018)\times10^{13}$ and $(2.650\pm0.018)\times10^{13}$, respectively. The number of ^{7}Be nuclei in the target after implantation $(t=0)$ was determined to be $n_t=(1.168\pm0.008)\times10^{16}$. In this evaluation, the branching ratio for γ emission in the decay of ^{7}Be was taken to be $(10.52\pm0.06)\%$ [29] and the half-life was taken as 53.29 ± 0.07 days [30]. The error on the branching ratio contributes the major fraction of the error on the total number of ^{7}Be nuclei.

E. Cross section measurement with a thin target of finite width

For a target of finite width, one has to account for the fact that the beam energy is spread over a finite range. For a thin target this can be accomplished by characterizing the target density distribution $\rho(x)$ by moments

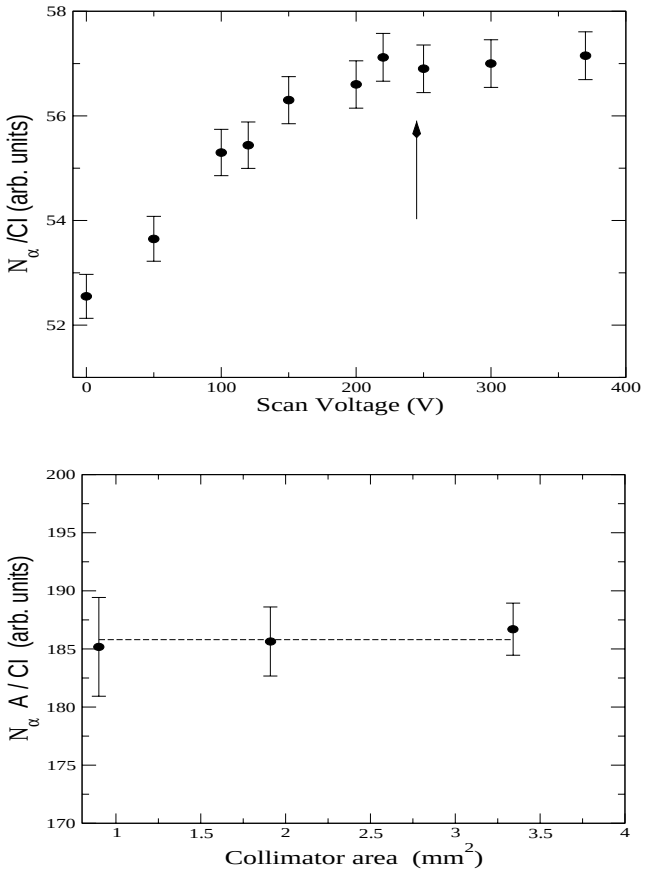

FIG. 5. Top: α yield from the ^{7}Li$(d,p)^8$Li reaction at $E_d=770$ keV, normalized to the integrated beam current as a function of the scan voltage. The scan voltage used in the experiment, scaled to the corresponding beam energy, is indicated by the marker. Bottom: α yield from the ^{7}Li$(d,p)^8$Li reaction for various collimators normalized to the integrated beam current and multiplied by the area of the collimator.

$$M_0=\int_{x_0}^{\infty}\rho(x)dx=n_t,$$

$$M_1=\frac{1}{n_t}\int_{x_0}^{\infty}x\rho(x)dx=\overline{x},$$

where $\overline{x}$ is the centroid and

$$M_2=\frac{1}{n_t}\int_{x_0}^{\infty}(x-\overline{x})^2\rho(x)dx.$$

The proton energy is related to the depth by

$$E=E_0-\kappa x,$$

where $\kappa=dE/dx$, which is assumed to be constant for a thin target.

The cross section σ close to some point x^* can be expanded in a power series,

TABLE I. The correction term to the cross section due to the second moment of the distribution. ϕ is defined in Eq. (6); Phase 1 and phase 2 refer to the periods before and after the thermal episode.

$E_{\text{c.m.}}$ (keV)	(dE_{lab}/dx) (eV/Å)	ϕ Phase 1	ϕ Phase 2
1078	9.6	-1.2×10^{-5}	-1.1×10^{-4}
850	10.9	-2.3×10^{-5}	-2.1×10^{-4}
415	15.7	-4.4×10^{-5}	-4.0×10^{-4}
356	16.0	$+2.2\times10^{-4}$	$+2.0\times10^{-3}$
302	17.0	$+7.1\times10^{-4}$	$+6.4\times10^{-3}$

$$\sigma[E(x)]=\sigma[E(x^*)]-[E(x)-E(x^*)]\kappa\sigma'[E(x^*)]+\frac{1}{2}[E(x)-E(x^*)]^2\kappa^2\sigma''[E(x^*)],$$

where $\sigma'(E)=d\sigma/dE$ and $\sigma''=d^2\sigma/dE^2$. The energy averaged cross section $\langle\sigma\rangle$ is given by

$$\langle\sigma\rangle n_t=\int_{x_0}^{\infty}\sigma(x)\rho(x)dx=\sigma[E(x^*)]n_t-\kappa\sigma'[E(x^*)]\times\int_{x_0}^{\infty}[x-x^*]\rho(x)dx+\frac{1}{2}\kappa^2\sigma''[E(x^*)]\times\int_{x_0}^{\infty}[x-x^*]^2\rho(x)dx\,.$$

If $x^*=\overline{x}$ and $\overline{E}=E(\overline{x})$, the second term vanishes and

$$\langle\sigma\rangle=\sigma(\overline{E})\left\{1+\frac{1}{2}\frac{1\kappa^2\sigma''(\overline{E})}{\sigma(\overline{E})}M_2\right\}. \tag{5}$$

According to Eq. (1),

$$\sigma(E)=S(E)\frac{1}{E}e^{-\sqrt{E_G/E}};$$

where $E_G=(2\pi e^2Z_1Z_2/\hbar c)^2/2$. Taking $S(E)$ to be constant for small energy intervals,

$$\langle\sigma\rangle=\sigma(\overline{E})\left\{1+\frac{1}{\overline{E}^2}\left(\frac{E_G}{\overline{E}}-7=\sqrt{\frac{E_G}{\overline{E}}}+8\gamma\right)\times\left(\frac{d\overline{E}_{\text{lab}}}{dx}\right)^2M_2\right\}(\sigma\overline{E}\{1+\phi\}. \tag{6}$$

For the simulated distribution of Fig. 3, $M_1=1220$ Å and $M_2=2.8\times10^5$ Å^2. The correction term ϕ is given in Table I for the relevant proton energies. In the ''thermal episode'' (see Sec. II J), M_2 was increased by a factor of 9. The appropriate values of ϕ are also given in Table I.

It is apparent that practically for all our measurements, $\langle\sigma\rangle=\sigma(\overline{E})$ is an adequate approximation. Only for the lowest energy, $E_{\text{c.m.}}=302$ keV, and the broadened M_2 following the thermal episode is there a small M_2 correction.

We now examine the resonance at $E_{\text{c.m.}}=633$ keV. We write the resonance equation in terms of the peak cross section $\sigma^r_{\max}$ and the width Γ, in the form

$$\sigma(E)=\frac{\sigma^r_{\max}}{1+\dfrac{4E^2}{\Gamma^2}};$$

taking the zero of the energy scale at the peak of the resonance,

$$\sigma''(E)=\frac{2}{\dfrac{\Gamma^2}{4}+E^2}\left\{\frac{\dfrac{4E^2}{\Gamma^2}}{\dfrac{\Gamma^2}{4}+E^2}-1\right\}\sigma(E),$$

σ'' has a sharp minimum at the maximum of the cross section at $E=0$ and we get from Eq. (5),

$$\langle\sigma\rangle_{\max}=\sigma^r_{\max}\left\{1-\frac{4\kappa^2}{\Gamma^2}M_2\right\}. \tag{7}$$

For $M_2=2.8\times10^5$ Å^2, $\kappa=12.3$ eV/Å, and $\Gamma=34$ keV, one obtains

$$\frac{4\kappa^2}{\Gamma^2}M_2=0.15. \tag{8}$$

From Eqs. (7) and (8), one can derive $\sigma^r_{\max}$ of the resonance from the measured $\langle\sigma\rangle_{\max}$.

F. The solid angle

The solid angle subtended by the detector at the ^{7}Be target was determined, as in Ref. [18], with the aid of the ^{7}Li$(d,p)^8$Li reaction on the ^{7}Li accumulated in the implanted target. The measurements were carried out in two steps.

(1) With a deuteron beam of $E_{\text{lab}}=770$ keV, the ratio of α counts to the integrated current $(N_\alpha/CI)_N$ was determined in the same geometrical conditions as in the ^{7}Be$(p,\gamma)^8$B measurement (geometry N).

(2) The detector was moved to a large distance from the target, h (geometry F), and a collimator of radius r was placed in front of it. The ratio $R=(N_\alpha/CI)_N/(N_\alpha/CI)_F=\Omega(N)/\Omega(F)$ was measured. With $h=95.7\pm0.1$ mm and $r=4.99\pm0.02$ mm, the solid angle $\Omega(F)$ was found to be $(8.520\pm0.02)\times10^{-3}$ sr, and from the measured ratio R the solid angle $\Omega(N)$ was evaluated.

These steps were carried out for each individual determination of the solid angle in close proximity in time (not more than 16 h between ''near'' and ''far'' measurements) and with no proton bombardment in between. These conditions were taken as an extra precaution even though we have determined experimentally the overall target stability, for both ^{7}Be and ^{7}Li (see Sec. II K).

As the α's are emitted in pairs with $\mathbf{p}(\alpha 1)+\mathbf{p}(\alpha 2)=0$, the efficiency for detecting a ^{8}Be α decay is twice the detection efficiency of α's, which is given by

$$\eta_{\mathrm{Be}}=\frac{2\Omega_\alpha}{4\pi}. \tag{9}$$

The ''near geometry'' measurements were carried out at four different target-detector distances of 7–10 mm. The detection efficiencies corresponding to the four geometries [numbered (1)–(4), respectively] used in the present experiment were $\eta_{\mathrm{Be}}(1)=0.1783$, $\eta_{\mathrm{Be}}(2)=0.2879$, $\eta_{\mathrm{Be}}(3)=0.2324$, and $\eta_{\mathrm{Be}}(4)=0.1752$.

To account for dead time, all α counts were referred to counts from a precision pulser. The system was checked by counting γ rays from a standard source at a standard distance with a secondary source at varying distances. In general, dead times were negligible for the $^7\mathrm{Be}(p,\gamma)^8\mathrm{B}$ measurements, whereas 1–3 % dead times were observed for most of the $^7\mathrm{Li}(d,p)^8\mathrm{Li}$ measurements. The highest dead times, up to 7%, were encountered in some of the near-geometry $^7\mathrm{Li}(d,p)^8\mathrm{Li}$ measurements.

The near-geometry measurements were also used to examine the overall consistency of the measurements. Every $\Omega(N)$ measurement consisted of five to seven individual high statistics measurements. These measurements indicated a fluctuation of $\pm$ 0.8%. Occasionally, larger deviations up to 2% were observed. These were all correlated with indications of detuning of the beam optical system and with an abrupt change in the beam ratio $R_b=$beam current (scan off/scan on) from a normal 5 to about 2. The value of $R_b=5$ is valid for both proton and deuteron beams, indicating that the size of the beam spot is similar. R_b was checked routinely to monitor the beam stability. A common error of $\pm 0.8\%$, obtained from the standard deviation of the set of $(N_\alpha/CI)_N$ and $(N_\alpha/CI)_F$ of the $^7\mathrm{Li}(d,p)^8\mathrm{Li}$ measurements, was applied to all individual measurements.

G. Background

There are four potential sources of background: detector noise, pileup noise from the $^7\mathrm{Be}\rightarrow{}^7\mathrm{Li}^*$ γ rays impinging on the detector, general background (no beam, no target), and multiply scattered protons. In our previous experiment [19] the detector was found to heat up in the presence of the target, leading to an increased noise level. In the present experiment the detector was water cooled, and the noise level was low and independent of the beam power input. The pileup noise is a prominent feature in the spectra, appearing as an almost vertical wall at the low-energy end. It is made up of high order coincidence events of very low energy pulses, generated by electrons that are created by the intense γ radiation from the ^{7}Be target. The position of the end point of the noise wall is very sensitive to the γ rate on the detector, and one observes a substantial retraction of the wall with time following the natural decay of the target, and with a reduced solid angle. The high statistics measurements (Fig. 6) exhibit good separation between the pileup wall and the α spectrum. These measurements were analyzed in detail and used as templates for the low count measurements.

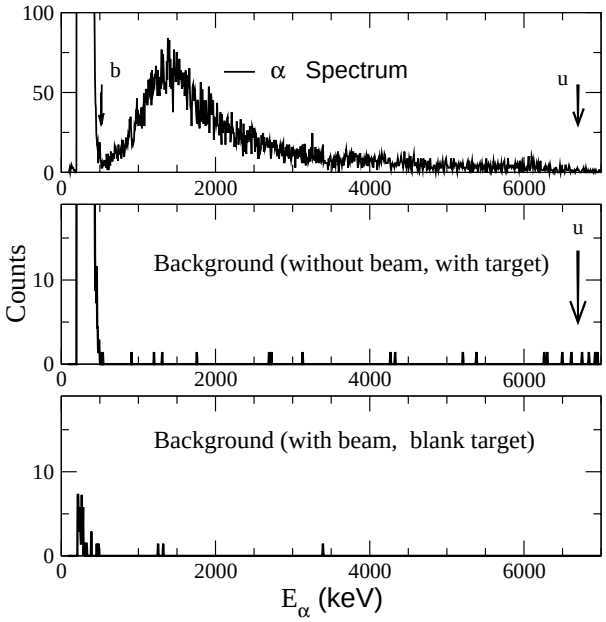

FIG. 6. Top: An α spectrum obtained at $E_{\mathrm{lab}}=991$ keV in the geometry (1). This spectrum was collected over a time of $\approx$40 hours. Middle: A background spectrum collected without beam and the target in front of the detector for a time of $\approx$33 h. The noise cutoff is at $E_\alpha\approx 525$ keV. Bottom: Background spectrum collected for a time of $\approx$5 h with the ^{7}Be target replaced by a copper blank.

The general background was measured off beam, with the target in position in front of the detector. Typical spectra are shown in Fig. 6. Above the pileup wall there is a roughly even distribution of counts, except for the high-energy end where the density is appreciably higher. The counts above the pileup wall are probably due to α's from (n,α) reactions in the detector or its close surroundings, and to α radioactivity in the same region. The excess of counts at the high-energy end of the spectrum is a saturation effect due to α's of sufficiently high energy to traverse the detector. The individual rates of the general background in the ''region of interest'' range from 0.4 to 0.6 ± 0.06/h.

The reaction chamber was constructed with tight antiscattering shields around the beam and around the target-detector assembly in the counting position. To get a measure of the scattered protons reaching the detector, we performed a number of background measurements in which the pileup noise was absent or reduced

(1) An in-beam measurement in the beam-on-target phase. In this case one expects an enhanced multiple scattering because the detector lacks the important shield provided by the extended target arm.

(2) An in-beam measurement with a reversed target.

(3) An in-beam measurement with a blank target.

In the third case the pileup noise is absent. In the first and second cases it is reduced because the γ rate at the detector is reduced due to the larger target-detector distance and the absorption in the copper.

In all these measurements the background level was found to be fully consistent with the off-beam level. Furthermore, the multiple-scattering events are expected to appear at the low end of the spectrum and to exhibit a sharp increase with decreasing energy. No such feature was observed (Fig. 6). The small peak at the low-energy end of the bottom panel of Fig. 6 is the tail end of the electronic noise. We therefore conclude that in our ''region of interest'' there are no multiple-scattering events.

H. Analysis of the spectra

Figure 6 shows a high statistics α spectrum at the geometry (1) together with a background spectrum. Above the marker ''u'' the number of counts in both spectra is nearly the same: 22 and 17, respectively. The difference is negligible compared to the total of $\approx 10^4$. The marker u was therefore adopted as the upper limit of the region of interest. A similar procedure was adopted for the spectra corresponding to geometries (1)–(4). At the lower end of the spectrum the dominant concern is the pileup wall. In a number of spectra the wall intercepts the ^{8}Be α spectrum at a fairly high-energy, and it is necessary to have a reliable extension of the α spectrum ''into the wall.'' For a very thin target and a small detector solid angle this is a straightforward task because the shape of the α spectrum is known [31]. Our target, however, has a finite thickness causing some energy loss of the α's, and the solid angle in some of the measurements is quite large so that the energy loss varies appreciably as a function of the α emission angle. For the evaluation of this region of the spectrum, we have adopted a procedure similar to the one described in Ref. [26]. The spectrum in Fig. 7 (top) reaches down to almost $N_\alpha = 0$ at the lowest energy, and we take this spectrum and some other high quality spectra, rather than the ''pure'' spectrum of Ref. [31], as models for the entire set of measurements. A Gaussian with an area equal to the integrated spectrum provides an excellent fit to the data from channel 280 down to the low end of the spectrum. The same is true for other high quality spectra, e.g., as in Fig. 7 (bottom), α's from ^{7}Li$(d,p)^8$Li at a near geometry for a deuteron energy of 398 keV where the ^{8}Li are located closer to the surface due to the lower deuteron momentum. We conclude that if a marker b is set at an energy higher than the pileup wall, a Gaussian fit to the region between markers b and i will provide an adequate extension to lower α energies.

The procedure for any given ^{8}B spectrum is to sum the counts between the b and u markers as presented in Fig. 6. The excess of α counts below the b marker is then derived from a Gaussian fit to the region: ''$b \rightarrow i$'' (see Fig. 7). The robustness of this procedure was verified with the aid of some high quality α spectra. The spectrum in the middle panel of Fig. 8, for example, was treated in this manner with b at various positions beyond the low-energy minimum, yielding N_α values that are well within the statistical errors. The ''tail corrections'' for the ^{8}B α spectra range from $(0.4 \pm 0.2)\%$ to $(1.0 \pm 0.6)\%$.

For the ^{8}Li α spectra, only the correction to the ratio $N_\alpha(\text{near})/N_\alpha(\text{far})$ is of significance. Figure 8 shows the far and near normalized α spectra for geometry (1). The Gaussian fits are essentially identical. The correction to $\eta_{\text{Be}}(N)/\eta_{\text{Be}}(F)$ due to tail correction can in this case be derived quite accurately, and is found to be $(0.8 \pm 0.5)\%$. At

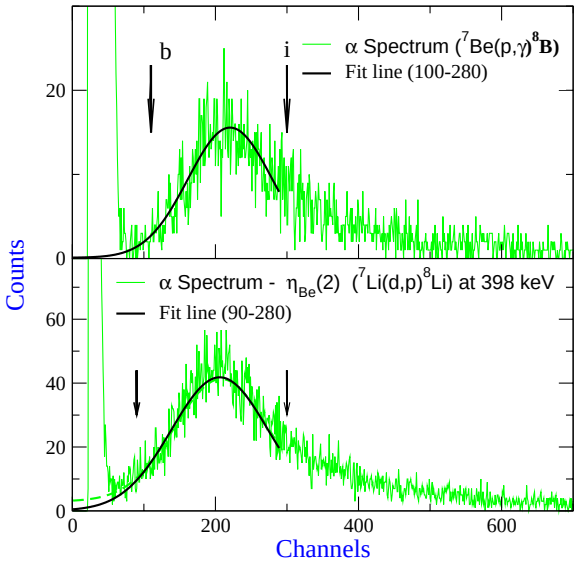

FIG. 7. Top: The α spectrum obtained from the ^{7}Be$(p,\gamma)^8$B reaction at 991 keV beam energy. The line is a Gaussian fit to the spectrum between the arrows marked ''b'' and ''i.'' Bottom: α spectrum obtained from the ^{7}Li$(d,p)^8$Li reaction for a deuteron energy of 398 keV. The Gaussian fit to the spectrum in the region between the arrows is shown by the line. In both spectra the extended low energy part of the fitted line agrees well with the low-energy tail of the α spectrum. The top panel spectrum was collected in the geometry (1), and the bottom one in geometry (2).

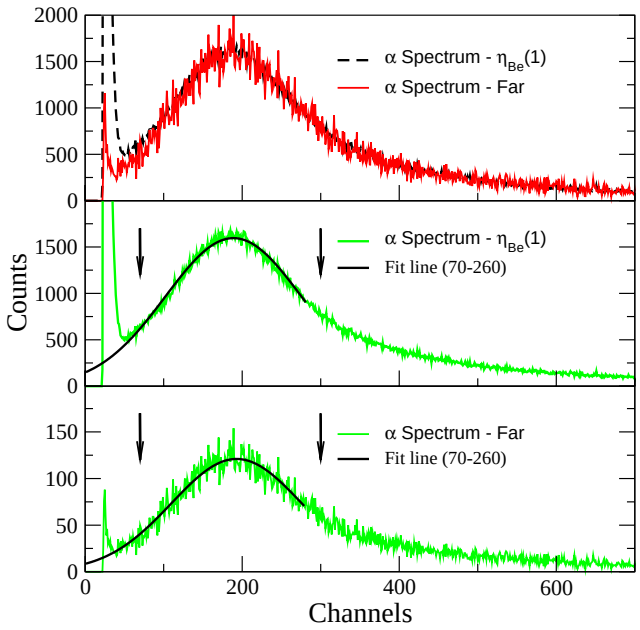

FIG. 8. Top: The α spectrum from the ^{7}Li$(d,p)^8$Li reaction for the near geometry (1) and the corresponding far geometry scaled to coincide at the peak. Middle and bottom: The individual α spectra and the respective Gaussian fits in the region between the markers.

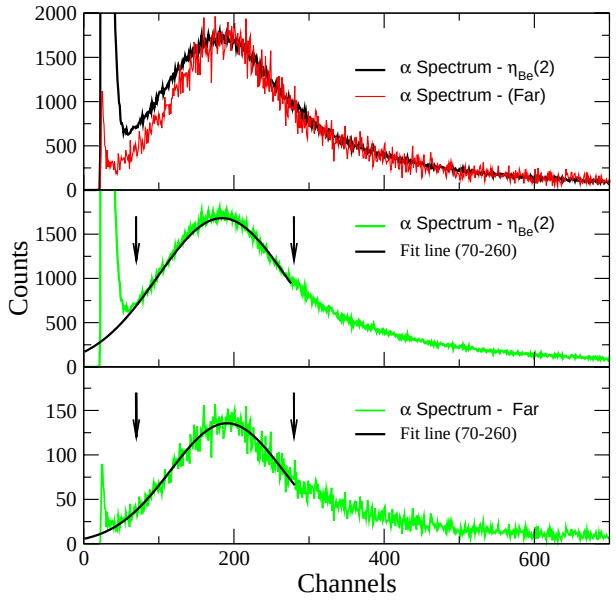

FIG. 9. Top: The α spectrum from the ^{7}Li$(d,p)^{8}$Li reaction at near geometry (2) and the corresponding far geometry scaled to coincide at the peak. Middle and bottom: The individual α spectra and the respective Gaussian fits in the region between the markers.

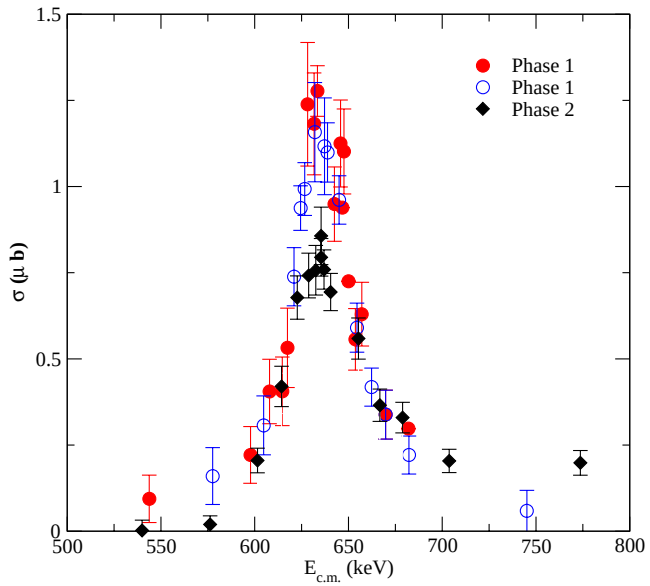

FIG. 10. Measurements around the 633 keV resonance in phase 1 and phase 2.

the other extreme, for the closest geometry (2), the Gaussian fits to the near and far spectra are different (Fig. 9) and the tail correction to the $\eta_{\mathrm{Be}}(N)/\eta_{\mathrm{Be}}(F)$ ratio is evaluated in this case as $(2.4\pm0.8)\%$. The fitted line has nonzero intercepts in some cases, indicating that there is a small fraction of the α's stopped in the target. For the ^{8}B measurements the error in the tail correction is always small compared to the statistical error. For the ^{8}Li measurements they constitute the dominant uncertainty.

I. The 633-keV *M*1 resonance

Measurements of the resonance were carried out repeatedly to establish and monitor the centroid (M_1) and the width (M_2) of the ^{7}Be depth distribution. The earliest of these measurements are shown in Fig. 10. The centroid shift of 15 keV confirms the centroid depth of the simulated distribution at 1215 Å. The value of $\sigma^{r}_{\mathrm{max}}$ can be inferred from the measured cross sectionat the peak and the value of M_2: 2.8×10^{5} Å^2 according to Eqs. (7), (8) yielding the value of $\sigma^{r}_{\mathrm{max}}=1340\pm100$ nb. In a more elaborate evaluation presented later in Sec. II K, the parameters of the resonance were determined as $\sigma^{r}_{\mathrm{max}}=1250\pm100$ nb and $\Gamma=35\pm3$ keV.

J. The thermal episode

At 350 h into the experiment, the ^{7}Be target underwent a ''thermal episode.'' A short experiment concerning the cross section of the reaction ^{7}Be$(^{3}$He$,2\alpha)2p$ was carried out with our ^{7}Be target at the Van de Graaff Laboratory [32]. In this experiment the target was not cooled sufficiently and the ^{3}He beam energy was dissipated by radiation. We estimate that the target reached a temperature of at least 400 °C. Following the event it was found that the ^{7}Be content of the target was reduced by a factor of 0.918 ± 0.003, the ^{7}Li content by 0.86, and the second moment of the ^{7}Be distribution was increased by a factor of 9. There was also an additional deposit of carbon of $\approx$3000 Å. These matters are discussed in detail below. The accuracy and reliability of the data were not affected by this, although the quality of the spectra at the low-energy end was impaired by the extra carbon deposit.

The fact that after such extreme heating the target was at all usable bears impressive evidence to the stability of the implanted target in both the ^{7}Be and ^{7}Li components. The temperature of the target was measured under conditions of normal usage and it was established that the target was never hotter than 110 °C. Of the 90 °C increase over room temperature, roughly half is due to the stepping motor to which the target is thermally connected, and the other half is due to the proton beam.

K. The target history

Absolute γ calibration measurements of the weak ^{7}Be target have been carried out a number of times (Fig. 11). They clearly point to a constant ^{7}Be inventory. There were a number of ''strong'' to ''weak'' comparisons, as well as regular γ monitoring measurements over an extended period (also shown in Fig. 11). It is apparent that the strong target also suffered no loss of ^{7}Be (other than in the thermal episode). The most likely cause of ^{7}Be loss is sputtering induced by the proton beam. The total proton charge into the target during the entire period of the measurement was about 1 C, and we can therefore infer that the proton-induced sputtering under the condition of our experiment is less than 1% per Coulomb. The ^{7}Li content can be inferred at the instance of every solid angle measurement from the value of N_{α}/CI, the known solid angle and the known cross section. Figure 12 shows the measured numbers of Li atoms fitted to a

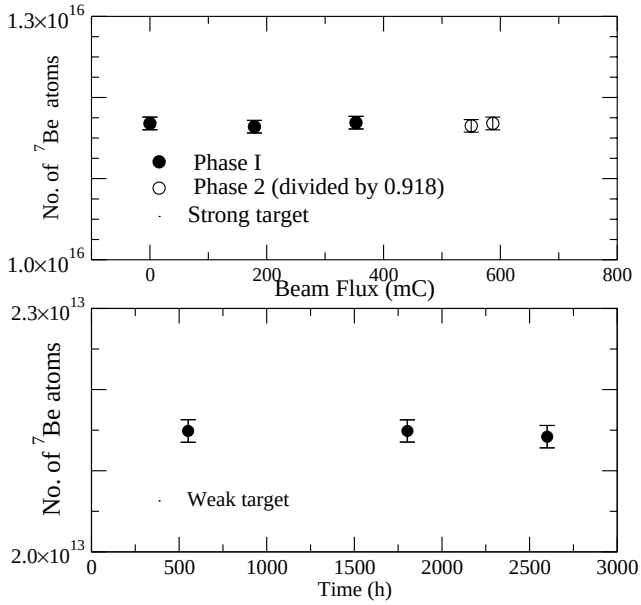

FIG. 11. Top: The ^{7}Be target content, determined by measuring the activity in a Ge detector, as a function of the accumulated charge on target and corrected for the decay of ^{7}Be. The open circles are scaled by a factor of 0.918 (see text). Bottom: The number of ^{7}Be atoms corrected for decay in the weak target as function of time.

curve, $n_{\mathrm{Li}}+n_{\mathrm{Be}}(1-2^{t/T_{1/2}})$, where n_{Li} and n_{Be} are the number of Li and Be atoms at the time of the target preparation. The good fit attests the stability of the ^{7}Li content.

Measurements in the resonance region were carried out routinely. Most were limited to the immediate neighborhood of the peak and were carried out with the aim of monitoring

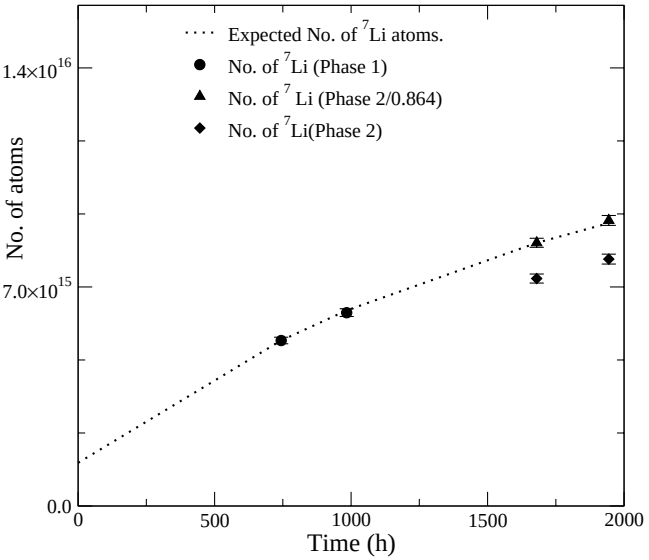

FIG. 12. The inventory of ^{7}Li atoms in the target. The number of ^{7}Li atoms was measured by the ^{7}Li$(d,p)^8$Li reaction. The circles represent the measured numbers in phase 1 and the triangles in phase 2, corrected for the fraction lost in the thermal episode. The line through the points represents the expected ^{7}Li accumulation due to the ^{7}Be decay.

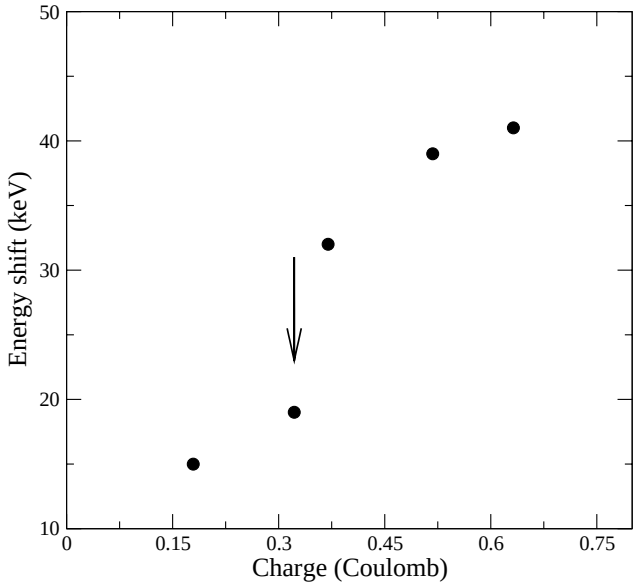

FIG. 13. The energy shift of the centroid of the 633-keV resonance due to carbon buildup on the target, as a function of the integrated charge. The marker indicates the "thermal episode" (see the text).

the centroid of the ^{7}Be distribution. Three measurements were carried out over a sufficient range to provide information also on the shape of the resonance. Figure 13 presents the shift of the resonance centroid as a function of time. Both the gradual shift and the large increase at the time of the thermal episode (at least most of it) are attributed to the carbon buildup. The three full resonance curve measurements are shown in Fig. 10. The first two are seen to be consistent. A fit to a pure resonance, modified by a target with the profile of Fig. 3 with $M_2=2.6\times10^5$ Å^2 is shown in the upper panel of Fig. 17. The resonance parameters extracted from this fit are $\sigma^r_{\mathrm{max}}=1250\pm100$ nb, σ_{max}(total) $=1560\pm120$ nb, and $\Gamma=35\pm3$ keV. Previously quoted values are $\sigma^r_{\mathrm{max}}=1180\pm120$ nb and $\Gamma=37\pm5$ keV [26]. The third resonance curve in Fig. 10, taken after the thermal episode, is clearly lower and broader. In this case M_2 was taken as a fit parameter and was found to be $M_2=2.34\times10^6$ Å^2.

III. THE ^{7}Be$(P,\gamma)^8$B MEASUREMENTS

The cross section is evaluated from Eq. (4). Cross section measurements were carried out at the energies of $E_{\mathrm{c.m.}}=1078$, 856, 415, 356, and 302 keV (where c.m. is the center of mass) and also around the 633-keV resonance. One of the major objectives of this work was to carry out a measurement at one proton energy as accurately as possible. This is important in order to serve as an accurate comparison between various (future) measurements. Such an experimental comparison is thus free of uncertainties related to the extrapolation procedure of $S_{17}(0)$. The energy $E_{\mathrm{lab}}=991$ keV has been chosen because this is the energy of the ^{27}Al$(p,\gamma)^{28}$Si resonance, the best calibration point. A number of measurements were carried out at this lab energy un-

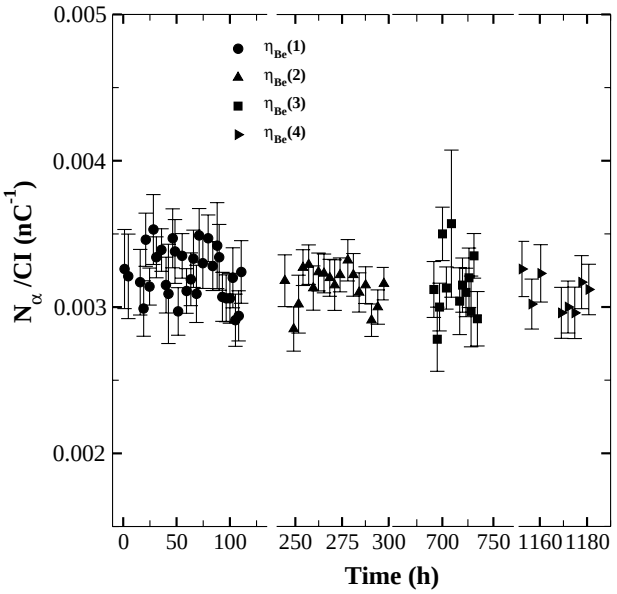

FIG. 14. The ratio of α counts to integrated current, N_α/CI, measured at the 991 keV beam energy as a function of time and normalized to the known decay rate of ^{7}Be, for various geometries of the α detector. The four symbols correspond to the measurements of points 2–5, respectively, in Table II. The measurements span over a period of more than 40 days.

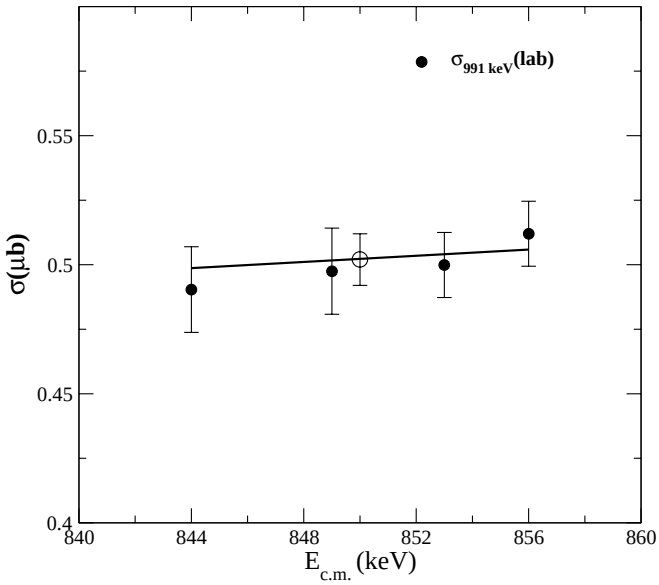

FIG. 15. The cross section for ^{7}Be$(p,\gamma)^8$B measured at different geometries at $E_{\rm lab}=991$ keV. The gradual energy shift is due to the carbon buildup on the target. The solid line is from Eq. (10). The open circle represents the average cross section at $E_{\rm c.m.}=850$ keV.

der varying conditions of solid angle and target strength, with slightly varying values of $E_{\rm c.m.}$, due to carbon buildup. The last two measurements were performed at a slightly higher energy, $E_{\rm lab}=998$ keV, to compensate for the carbon buildup in the thermal episode. The measurements were carried out before and after the thermal episode, and extended altogether over a period of 40 days. The four energy points also demonstrate the relative stability of the measurements in the two phases. The individual runs are shown in Figs. 14 and 15 and the cross section values are presented in Fig. 15 together with a fit to the function:

$$S_{17}\ (850\ \text{keV})\frac{1}{E_{\rm c.m.}}e^{-\sqrt{E_G/E_{\rm c.m.}}}. \qquad (10)$$

The combined value of S_{17} at this point is $S_{17}(850\ \text{keV})=24.0\pm0.5$ eV b. Another measurement, at $E_{\rm c.m.}=1078$ keV, was carried out in phase 1, and three measurements at lower energies at 415, 356, and 302 keV in phase 2. These are presented in Table II.

Practically for all the measurements the target can be considered thin even in the broadened state of phase 2, in the sense that the integration over the density distribution amounts to correlating the cross section measurement with the proton energy at the centroid of the ^{7}Be distribution. Only for the 302-keV measurement does the second term in Eq. (6) have a barely significant value of 0.6%. The centroid energy was determined in every instance directly for the ^{7}Be$(p,\gamma)^8$B resonance by measuring the energy shift of the peak. This shift was then reevaluated for the relevant energies in specific measurements by applying the appropriate dE/dx factors. For this, one needs to know separately the amount of C and Cu in the proton path. We have assumed that the centroid of ^{7}Be distribution in the copper did not change, and that any additional energy loss is due to C deposition. This assumption is well supported for phase 1, but not so well for phase 2. Even though there is evidence that a large part of the energy loss is indeed in carbon, we consider as a limit the possibility of ''only Cu'' for the extra energy loss. This yields for the lowest proton energy, $E_{\rm c.m.}=302$ keV, a reduction in loss of 5 keV, a corrected energy $E_{\rm c.m.}=307$ keV, and a decrease in $S_{17}(E)$ of 3.7%. We have chosen to leave the ''only C'' value unchanged and enlarged the error from 9% to 10% to cover the unlikely eventuality. For the higher proton energies an only Cu assumption does not change the quoted values and errors.

The quoted errors in Table II are made up of (in %) target activity (^{7}Be content): 0.7, background correction: 0.1–1.2, solid angle: 0.8–1.4, α spectrum cutoff: 0.3–0.8, beam collimator area: 0.8, time sequence efficiency: 0.2, and the uncertainty due to the proton energy calibration: 0.2–1.0. The high-energy points were measured with statistical precision varying from 1.0–1.8 and the points below the resonance with (4.0–8.0)%.

IV. RESULTS AND DISCUSSION

The results of this work are presented in Table II in term of $S_{17}(E)$ values. The ultimate goal of cross section measurement is to evaluate the cross section at solar energies, and the experimental determination of the cross section in the region of the Gamow peak was and remains paramount; this goal has not been achieved yet. The alternative is to measure the cross section at higher energies and employ theoretical models for the extrapolation to solar (''zero'') en-

TABLE II. The measured $S_{17}(E)$ values along with the details of the estimated error. The * indicates the set of measurements carried out at $E_{\text{c.m.}}$ close to 850 keV; the slightly different values of $E_{\text{c.m.}}$ are due to gradual carbon buildup, monitored by repeated measurements of the resonance. A combined value of the measurements near $E_{\text{c.m.}}=850$ keV, using Eq. (10), is also given. Points indicated by ** were measured after the thermal episode as described in the text. Columns 3–7 represent the contributions to the error from counting statistics, background, beam energy, correction for α loss below the region of interest, and a set of common errors. The error on the number of ^{7}Be atoms, solid angle, timing efficiency, and the area of the beam collimator.

$E_{\text{c.m.}}$ (keV)	S_{17}(E) (eV b)	Statistical	Background	Energy	α Cutoff	Common
1078	25.5 ± 0.8	0.49	0.03	0.08	0.20	0.52
856*	24.3 ± 0.6	0.29	0.03	0.07	0.08	0.45
853*	23.8 ± 0.6	0.24	0.03	0.07	0.08	0.48
849*	23.8 ± 0.8**	0.44	0.03	0.10	0.08	0.54
844*	23.6 ± 0.8**	0.54	0.03	0.10	0.14	0.44
415	20.2 ± 1.5**	1.36	0.16	0.36	0.06	0.45
356	18.8 ± 1.1**	0.90	0.19	0.37	0.06	0.42
302	18.1 ± 1.8**	1.50	0.21	0.80	0.06	0.40
850	24.0 ± 0.5					

ergy. Several models have been proposed for the extrapolation of the cross section to zero energy. A detailed discussion of the various models is given by Jennings *et al.* [33], where it is shown that the various models coalesce at center-of-mass energies below $\approx$400 keV and that, in general, cluster models fit the experimental data up to $\approx$1.2 MeV. The practice of employing a generally adopted extrapolation model is supported by the observation that the disagreements among experiments are mostly in factors of proportionality in the cross section while the measured energy dependence is largely consistent. We have put this general observation to a quantitative test: in Fig. 17 the nonresonant part of the $S_{17}(E)$ values from recent measurements are shown with each set of values fitted separately to the DB model by a scaling constant to yield an extrapolated value of $S_{17}(0)=21.2$ [this value has been chosen arbitrarily to match with the $S_{17}(0)$ from the present measurement]. The dashed line drawn through the data points is a Descouvmont-Baye (DB) fit to the entire set with a normalized χ^2 of 1.08. The energy dependence of all measurements is clearly similar and, in turn, fully consistent with the DB model. The red and blue lines are separate fits to the region above and below 400 keV, that agree to better than 1%. We conclude that to the precision of the present experiments, the DB model provides a representation of the measured cross sections (applying the individual renormalization factors as discussed above) up to at least 1.2 MeV, that is as good as the ''universal'' fit of all models to the region below 400 keV.

For the extraction of $S_{17}(0)$ value from our measurements, we have adopted a procedure of including all measurements, off and on the resonance, in a fit with the values of $\sigma_{\max}$ and Γ of the resonance and the overall normalization of the Descouvemont-Baye theory as free parameters (Fig. 16). We arrive in this way at a value of $S_{17}(0)=21.2\pm0.7$ eV b. We also quote for completeness the value derived from the low energy points (below the resonance) only as $S_{17}(0)=20.8\pm1.3$ eV b.

Table III gives the $S_{17}(0)$ values of the most recent publications of direct capture reactions with a radioactive ^{7}Be target. Included here are the recent precise measurements (taking note *inter alia* of the possibility of backscattering loss). From Table III we arrive at a mean value: $S_{17}(0)=21.1\pm0.4$ eV b with $\chi^2/\nu=2.0$ suggesting some discrep-

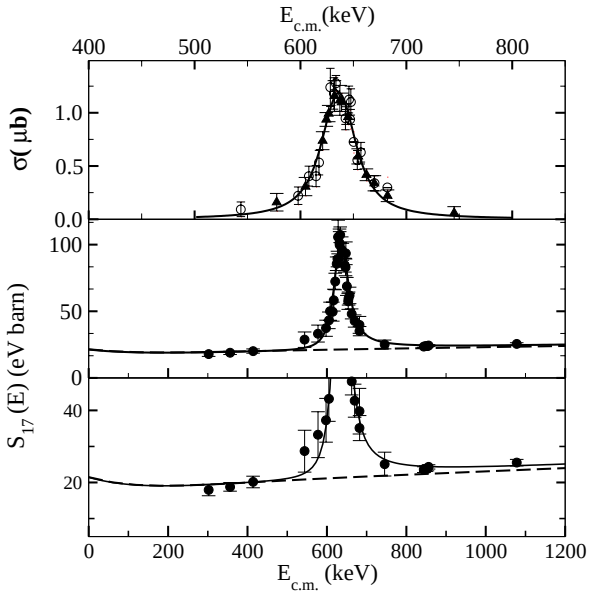

FIG. 16. Top: The resonance at 633 keV. The points are the measured cross sections after subtraction of the nonresonant part. The energy axis is expanded in comparison to the middle and lower panels. The two symbols represent two separate measurements. The continuous curve represents the convolution of a Breit-Wigner resonance with the simulated ^{7}Be distribution in Cu. Middle: The points are the measured $S_{17}(E)$. The continuous line is the scaled function of Descouvemont and Baye (DB) [34] plus a Breit-Wigner resonance with an energy-dependent width. The dashed line is the scaled DB model. Bottom: An expanded view of the middle figure.

TABLE III. A compilation of the $S_{17}(0)$ values from recent direct capture measurements.

Experiment	$S_{17}(0)$(eV b)
Hammache *et al.* [20]	18.8 ± 1.7
Strieder *et al.* [22]	18.4 ± 1.6
Hass *et al.* [19]	20.3 ± 1.2
Junghans *et al.* [21]	22.3 ± 0.7
Present	21.2 ± 0.7

ancy. If we omit the value of Ref. [21] (which is being revised) from the list, we get a consistent mean value: $S_{17}(0) = 20.5 \pm 0.5$ eV b with $\chi^2/\nu = 1.2$. If we add to this in quadrature an "error in theory" of (± 0.5), as suggested in Ref. [21], we get a consistent common value: $S_{17}(0) = 20.5 \pm 0.7$ eV b.

When relating this value to the environment of the solar interior, one is faced with two inherent uncertainties related to the extrapolation of the cross section to the solar energy region and to the atomic screening correction. The ± 0.5 eV b uncertainty quoted above from Ref. [21] is an attempt to quantify the first, and the second one is believed to be small [1].

The predicted ^{8}B neutrino flux $\phi(^8\mathrm{B})$ is directly proportional to $S_{17}(0)$. If the average value of $S_{17}(0)$ quoted above is introduced into the standard solar model [35], replacing the presently adopted value of $S_{17}(0) = 19^{+4}_{-2}$ [1], the uncertainty in $S_{17}(0)$ will become insignificant compared to other sources of error in the evaluation of $\phi(^8\mathrm{B})$ [36].

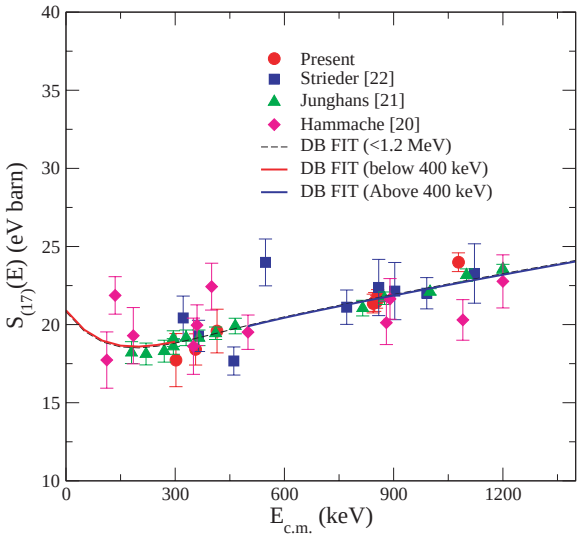

FIG. 17. (Color) Nonresonant part of the $S_{17}(E)$ from recent direct capture measurements. Each set of $S_{17}(E)$ values was fitted independently to the DB parametrization, and the individual scaling factors were then renormalized to a reference value corresponding to $S_{17}(0) = 21.2$ eV b. The overall consistency of the data up to $E_{\mathrm{c.m.}} = 1.2$ MeV as well as the agreement with the DB parametrization is apparent.

ACKNOWLEDGMENTS

We wish to thank the technical staff of the ISOLDE (CERN), PSI, and Y. Shachar and the technical staff of the Accelerator Laboratory of the Weizmann Institute. We acknowledge with gratitude the help of J. C. Hardy and V. E. Iacob with the intensity calibration of the ^{7}Be target. We thank Professor K. A. Snover for a fruitful exchange of information regarding the results of Ref. [21] and work in progress. This work was supported in part by the Israel-Germany MINERVA Foundation.

[1] E.G. Adelberger *et al.*, Rev. Mod. Phys. **70**, 1265 (1998).
[2] J.N. Bahcall, P.I. Krastev, and A.Yu. Smirnov, Phys. Rev. D **58**, 096016 (1998).
[3] S. Fukuda *et al.*, Phys. Rev. Lett. **86**, 5656 (2001).
[4] Q.R. Ahmad *et al.*, Phys. Rev. Lett. **87**, 071301 (2001); **89**, 011301 (2002).
[5] G. Fiorentini and B. Ricci, Phys. Lett. B **526**, 186 (2002).
[6] V. Barger, D. Marfatia, and K. Whisnant, Phys. Rev. Lett. **88**, 011302 (2002).
[7] I.P. Lopes and J. Silk, Phys. Rev. Lett. **88**, 151303 (2002).
[8] R. Davis, Prog. Part. Nucl. Phys. **32**, 13 (1994).
[9] F. Terrasi *et al.*, Nucl. Phys. **A688**, 539c (2001).
[10] T. Kikuchi *et al.*, Eur. Phys. J. A **3**, 213 (1998).
[11] N. Iwasa *et al.*, Phys. Rev. Lett. **83**, 2910 (1999).
[12] B. Davids *et al.*, Phys. Rev. C **63**, 065806 (2001).
[13] H.M. Xu *et al.*, Phys. Rev. Lett. **73**, 2027 (1994).
[14] A. Azhari *et al.*, Phys. Rev. C **63**, 055803 (2001).
[15] L. Trache, F. Carstoiu, C.A. Gagliardi, and R.E. Tribble, Phys. Rev. Lett. **87**, 271102 (2001).
[16] B.A. Brown, P.G. Hansen, B.M. Sherrill, and J.A. Tostevin, Phys. Rev. C **65**, 061601(R) (2002).
[17] T. Motobayashi, Nucl. Phys. **A693**, 258 (2001).
[18] L. Weissman *et al.*, Nucl. Phys. **A630**, 678 (1998).
[19] M. Hass *et al.*, Phys. Lett. B **462**, 237 (1999).
[20] F. Hammache *et al.*, Phys. Rev. Lett. **86**, 3985 (2001).
[21] A.R. Junghans *et al.*, Phys. Rev. Lett. **88**, 041101 (2002). The cross section values of this paper are currently being revised; K. A. Snover (private communication).
[22] F. Strieder *et al.*, Nucl. Phys. **A696**, 219 (2001).
[23] L.T. Baby *et al.*, Phys. Rev. Lett. **90**, 022501 (2003).
[24] L. Weissman, M. Huyse, P. Van den Bergh, and P. Van Duppen, Nucl. Instrum. Methods Phys. Res. A **452**, 147 (2000).
[25] L. Weissman, M. Hass, and V. Popov, Nucl. Instrum. Methods Phys. Res. A **400**, 409 (1999).
[26] B.W. Filippone *et al.*, Phys. Rev. C **28**, 2222 (1983).
[27] U. Köster *et al.*, Report EMIS-14, 2002; Nucl. Instrum. Methods Phys. Res. B **204**, 343 (2003).
[28] J.C. Hardy *et al.*, Appl. Radiat. Isot. **56**, 65 (2002).

[29] See S. Y. F. Chu, L. P. Ekstrom, and R. B. Firestone, nucleardata.nuclear.lu.se/nucleardata/toi/
[30] *Nuclear Wallet Cards*, 6th ed., edited by J.K. Tuli (National Nuclear Data Center, Upton, NY, 2000).
[31] E.K. Warburton, Phys. Rev. C **33**, 303 (1986).
[32] R. H. France *et al.*, Nucl. Phys. **A718**, 398c (2003).
[33] B.K. Jennings, S. Karataglidis, and T.D. Shoppa, Phys. Rev. C **58**, 3711 (1998).
[34] P. Descouvemont and D. Baye, Nucl. Phys. **A567**, 341 (1994).
[35] J.N. Bahcall, M.H. Pinsonneault, and S. Basu, Astrophys. J. **555**, 990 (2001).
[36] J.N. Bahcall, astro-ph/0209080.